GROOVE-PATTERNS EFFECTS ON MIXING PERFORMANCE IN A MICRO-MIXER

K. Tatsumi, Y. Tsukanaka and K. Nakabe

Department of Mechanical Engineering, Osaka Prefecture University, Sakai, Osaka 599-8531, JAPAN

ABSTRACT

The performances of the block-inserted and groove-embedded rectangular ducts are investigated in the meaning of enhancing the fluid mixing under very low Reynolds number conditions. Both numerical and experimental studies have been carried out to discuss the block and groove pattern effects on the mixing characteristics and to evaluate the numerical scheme and experimental procedure. The results obtained by the two approaches agreed fairly well with each other in a qualitative manner. By applying the block and groove to the channel, a higher mixing rate was obtained in a shorter length compared to a smooth rectangular duct. The grooved channel was effective even in the channels with large aspect ratio. A better mixing was achieved with the case of asymmetric pattern than the symmetric case. The difference of the groove width also changed the flow and mixing characteristics, however, the total performance eventually did not differ much. At the end of this paper, the performances of the hook-type groove case and the oblique groove case are compared.

INTRODUCTION

The development of the Micro Electro Mechanical System (MEMS) technology in the past few decades has risen the feasibility of miniature-sized devices into which multiple functions are integrated, so-called Lab-on-a-Chip or Micro Total Analysis Systems (μ-TAS). The scale of flow channels in such devices is in the range of 10 ~ 100μm which accompanies a large decrease of the Reynolds number and incurs a serious deterioration of fluid mixing. Therefore, various techniques have been studied based on both passive and active ways for purposes to effectively enhance the mixing. In the present article, several types of micro-channels of different geometry were studied here as a passive technique: such as block inserted channels or channels with grooves embedded at the bottom wall. The velocity and concentration profiles in these channels are examined in order to provide some hints for designing an effective micro-mixer. These kinds of relatively simple structures can be easily fabricated by using etching process or micro- and nano-printing processes which enables cost saving of the products.

Geometric conditions of the channel, block and groove, such as channel aspect ratio, groove width or symmetric and asymmetric patterns, were varied and their effects were examined by both experimental and numerical approaches. In the numerical study, three-dimensional computation was conducted for the flow and concentration fields under laminar and incompressible flow conditions. In the experiment, the fluid velocity profiles were measured using a micro Particle Image Velocimetry (μ-PIV) system. The concentration was estimated from the data obtained through two types of measuring methods: one is by counting fluorescent tracer particles fed into the flow, and the other is by detecting the luminance intensity of fluorescent dye mixed in the fluid.

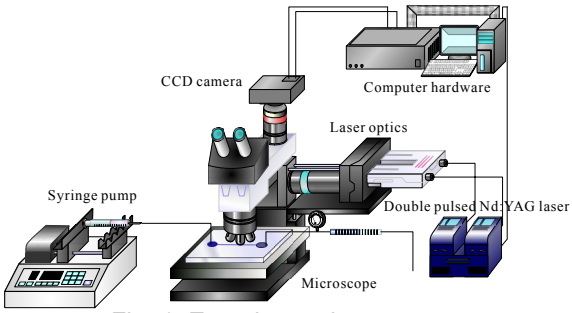

Fig. 1. Experimental apparatus.

Numerical Procedure

Finite-Volume Method (FVM) is adopted in the present three-dimensional numerical computation. The governing equations of the flow solved in this study are continuity and Navier-Stokes equations. These equations are described in time-dependent, incompressible form and are shown as follows:

$$\frac{\partial U_i}{\partial x_i} = 0 \tag{1}$$

$$\rho \frac{DU_i}{Dt} = -\frac{\partial P}{\partial x_i} + \frac{\partial}{\partial x_j}\left(\mu \frac{\partial U_i}{\partial x_j}\right) \tag{2}$$

where U_i is the velocity of x_i direction. ρ and μ are the fluid density and viscosity, respectively.

To discuss the mixing performance of the channels, the following equation of concentration conservation of binary mixture is also calculated in the present computation.

$$\rho \frac{Dc}{Dt} = \frac{\partial}{\partial x_i}\left(\frac{\mu}{Sc}\frac{\partial c}{\partial x_i}\right) \tag{3}$$

Here c is the mixture fraction of ethanol in water. Sc is the Schmidt number and the value applied in the present computation is Sc=657, which represents the diffusion between ethanol and water.

In the discretization method, 4th-order central-difference scheme is employed for the diffusion terms and the 5th-order upwind scheme is employed for the convective terms. These higher order schemes are applied in the present code to reduce the discretization errors, particularly numerical diffusion errors. However, in solving Eq. (3), 1st-order upwind scheme and 2nd-order central-difference scheme are respectively applied to the convective and diffusion terms to reduce the computational load. A modified version of the Semi-Implicit Method for Pressure-Linked Equations algorithm (SIMPLEC) is applied to solve the pressure correction. To solve the discretized equations, a linear-iterative method using the modified Tri-Diagonal Matrix Algorithm (TDMA) combined with an Alternating Direction Implicit Method (ADI) is employed.

Experimental Procedure

Figure 1 shows the experimental apparatus of the μ-PIV system which is applied in the present study to measure the velocity of the flow in the micro-channel. An Nd-YAG

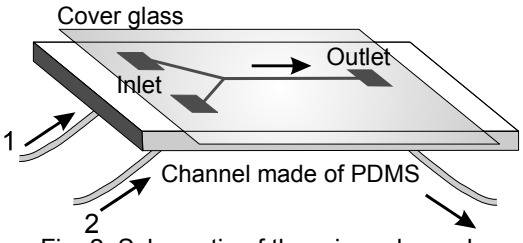

Fig. 2. Schematic of the micro-channel.

laser (2nd harmonic wavelength=532nm) is connected to a microscope, through which the laser is emitted to the targeted channel. Fluorescent micro spheres (Duke Scientific Corporation R820: radius=0.82μm) are mixed in the flow as tracer particles and the fluorescence is recorded by a high resolution CCD camera (TSI Powerview 4M). The objective lens used in the present study has a magnification of 40 and numerical aperture of NA=0.75. The focal depth calculated by the following equation will be, therefore, Δy=5.7μm [1].

$$\Delta y \cong \frac{3n\lambda}{NA^2} + \frac{2.16d_p}{tan\theta} + d_p \qquad (4)$$

n is the refraction index of the fluid located between the lens and the cover glass, λ is the wavelength of the light, and θ is 1/2 of the apex angle of the cone defined between the fluorescent particle and the objective lens. d_p is the diameter of the fluorescent tracing particle. Δy becomes the spatial resolution in the depth direction of the measured cross-sectional flow field. The optical spatial resolution of the microscope calculated by the following equation is α=0.41μm.

$$\alpha = \frac{\lambda}{2NA} \qquad (5)$$

Note that this value is larger than the CCD camera resolution, 0.18μm.

The schematic view of the micro-channel test section is shown in Fig. 2. A cover glass is attached to the upper side of the channel and the fluorescence of the particles is recorded from this side. The channel is made of PDMS (poly-dimethylsiloxane) and is fabricated by using SU-8 (MicroChem Co.) as a mold. This SU-8 mold is made by an etching process. First a mask on which the groove patters are printed is prepared by using an enlarger (Fujifilm FD-690) and a high precision photo plate (HRP-SN-2 2.5X2.5 30Z). Then, through this mask, the SU-8 layer is exposed to the UV light and the channel pattern is printed on the layer. After the post baking and etching processes, an SU-8 mold is completed. PDMS in liquid is then poured over the SU-8 mold, and is hardened and ripped off.

A Y-junction type channel shown in Fig. 2 is used in the experiment to discuss the mixing performance of each channel. Two kinds of measurements were conducted to evaluate the mixing characteristics at the test section. One is by feeding fluid containing the aforementioned fluorescent particles from one side of the Y-junction (inlet #2 in Fig. 2). In this case, the mixing rate is obtained by calculating the number density of the particles in the channel. The other is by feeding fluid containing Rhodamine B, again from one side of the header. In this case, the mixing rate is obtained by measuring the fluorescence intensity and applying it to the linear function calibrated by a preliminary experiment.

Table 1. Conditions for block-inserted channels.

	h/H	*w*/H	*L*/H	*AR*(=W_d/H)	*Re*
Case-B1	0.4	0.5	3.0	1.0	3.0
Case-B2	0.4	1.0	3.0	2.0	2.0
Case-B3	0.4	1.5	3.0	3.0	1.0

Table 2. Conditions for grooved channels.

	d/H	*w*/H	*b/H*	*L*/H	*AR*	*Re*
Case-SHG	1.0	1.0	1.0	3.0	3.0	1.5
Case-AHG2	1.0	1.0	1.0	3.0	2.0	2.0
Case-AHG3	1.0	1.0	1.0	3.0	3.0	1.5
Case-AHG4	1.0	1.0	1.0	3.0	4.0	1.2
Case-AHG3b	1.0	1.0	3.0	3.0	3.0	1.5

Table 3. Experimental conditions.

	d/H	*w*/H	*b/H*	*L*/H	*AR*	*Re*
Case-AHGE	0.7	0.6	0.7	2.2	2.2	1.5
Case-AOGE	0.7	0.6	1.3	5.0	2.2	1.5

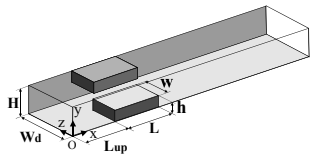

(a) Block-inserted case

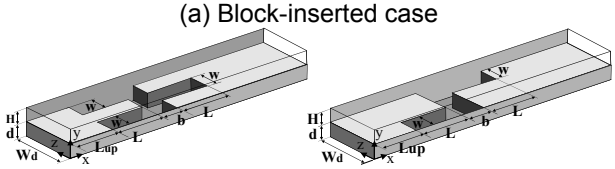

(b) Symmetric groove case (c) Asymmetric groove case

Fig. 3. Computational domain.

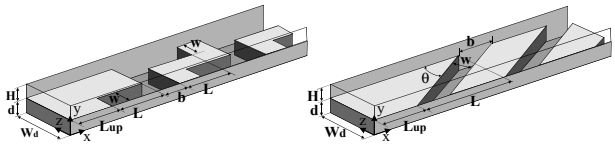

(a) Asymmetric hook type groove (b) Oblique groove

Fig. 4. Test section of the experiment.

Although the former case only shows the contribution of the convection to the concentration field, one can obtain a cross-sectional view of the field in the depth direction due to the same principle of the flow field measured by the μ-PIV.

Numerical and Experimental Conditions

Figure 3 illustrates the computational domain of the block-inserted and grooved channel cases. In the block case, blocks are attached diagonally to the top and bottom walls. In the grooved channel case, the groove is applied only at the channel bottom wall, and two types of groove patterns are studied, i.e. symmetric and asymmetric cases. The geometric conditions examined in the block-inserted and grooved channel cases are tabulated respectively in Table 1 and 2. The flow rate and channel height, H, are kept constant in all cases, and Reynolds number, which is based on the channel hydraulic diameter, differs when the channel aspect ratio is changed. At the inlet boundary, a uniform velocity flow is assumed to enter the computational domain. For the concentration field, the values of mixture fractions of c=0 and 1 are applied respectively to each half side divided by the channel centerline. L_{up} shown in Fig. 3 is the distance between the

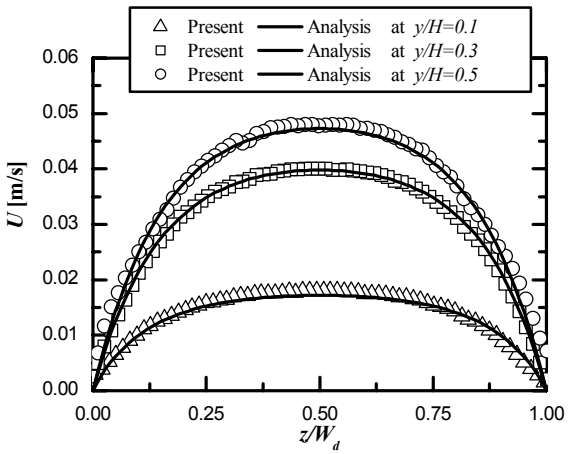

Fig. 5. Time-mean velocity distributions in a rectangular duct.

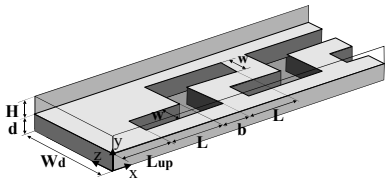

Fig. 6. Test section of preliminary test case.

inlet and the blocks or grooves, and is constant as L_{up}=5.0 for all cases. By the time the flow reaches the block-inserted or grooved area, a certain amount of diffusion between the two fluids is expected. Compared to the mixing produced by the blocks and grooves, however, the mixing ratio in this area is considered to be relatively small.

The groove patterns examined in the experiment are shown in Fig. 4. In this case, the flow and mixing characteristics of a channel with asymmetric hook-type grooves same as Fig. 3(c), and oblique grooves are discussed. 30 grooves are periodically embedded in the wall and the streamwise pitch, p, in both cases are p/H=3.8. The geometric conditions of the channel are shown in Table 3. Due to the fabrication process, to create a channel of exact same condition with the numerical study is difficult. Therefore the conditions shown in Table 2 and 3 are not exactly the same.

RESULTS AND DISCUSSION

Preliminary Test Cases for Evaluation of the Numerical and Experimental Procedures

In this section, discussion is made on the results of a preliminary test to evaluate the numerical and experimental procedures applied in the present study. Two cases are shown here, i.e. a comparison of the μ-PIV measurement and theoretical analysis of viscous flow of a smooth rectangular channel, and a comparison between the numerical and experimental results for the flow in a grooved channel.

Figure 5 shows the cross-sectional distributions of the streamwise velocity U measured at y/H=0.1, 0.3 and 0.5 of a rectangular smooth channel case. The abscissa is the spanwise location normalized by the channel width, W_d, which is approximately 200μm. The channel aspect ratio is 2.2. The Reynolds number based on the channel hydraulic diameter is Re=3.0. For comparison, the results of a three-dimensional theoretical analysis in a rectangular channel [2] are included in the figure as the

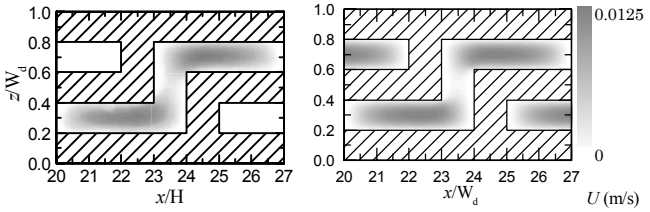

(a) Experiment (b) Numerical simulation

Fig. 7. Comparison of streamwise velocity distributions in x-z plane at y/H=0.26 (inside the groove).

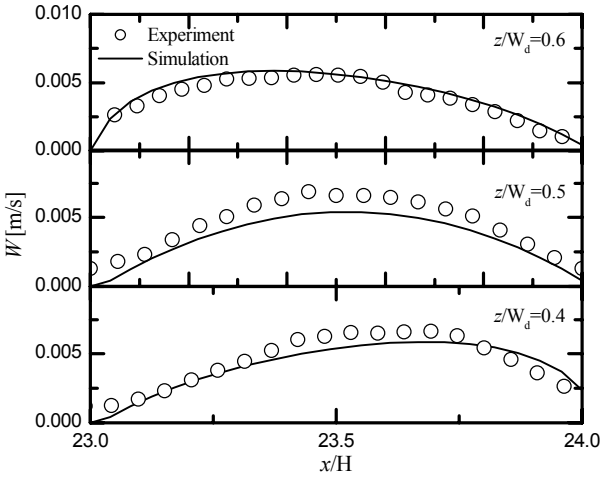

Fig. 8. Comparison of the cross-sectional profile of the spanwise velocity at z/W$_d$=0.4, 0.5, 0.6.

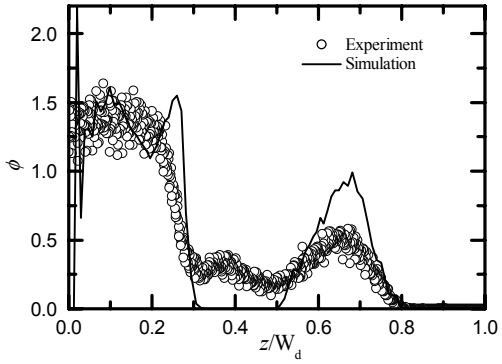

Fig. 9. Comparison of the apparent mixture fraction, ϕ.

solid lines. The experimental results agree well with the theoretical ones indicating that an accurate measurement of the three-dimensional velocity distribution is performed using the present experimental apparatus.

Next, comparison of the velocity and mixture fraction fields obtained by the numerical computation and experiment is carried out for the grooved channel. The test section discussed here is shown in Fig. 6. In this preliminary test, the channel width is larger than the groove total spanwise width. This will reduce the groove effect on the flow and mixing characteristics. However, the geometric error due to the channel fabrication process, such as the alignment of the mask, is reduced as well, and a more accurate comparison with the numerical computation is possible. The geometric conditions of the groove is same as those shown in Table 2 for both experimental and numerical cases, except that the channel aspect ratio and groove streamwise pitch are AR=W_d/H=5.0 and p/H=5.0. The numbers of the

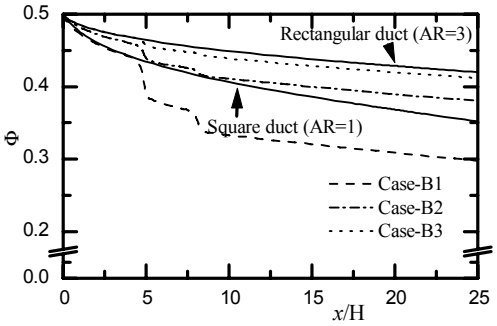

Fig. 10. Comparison of unmixed rate, Φ, of block inserted case.

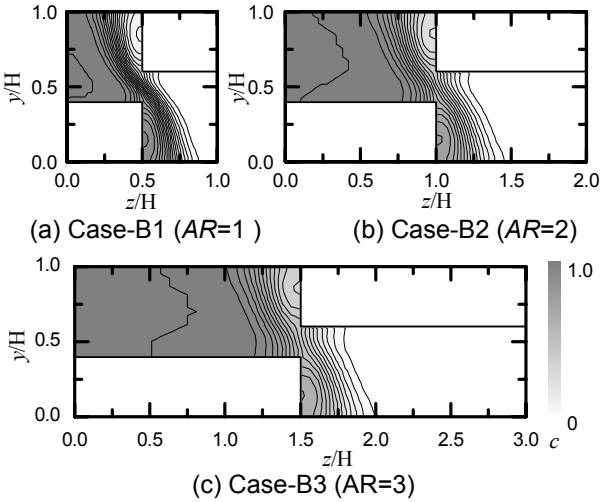

(a) Case-B1 (*AR*=1) (b) Case-B2 (*AR*=2)

(c) Case-B3 (AR=3)

Fig. 11. Mixture fraction contours in *y*-*z* plane at *x*/H=6.5 (block inserted case).

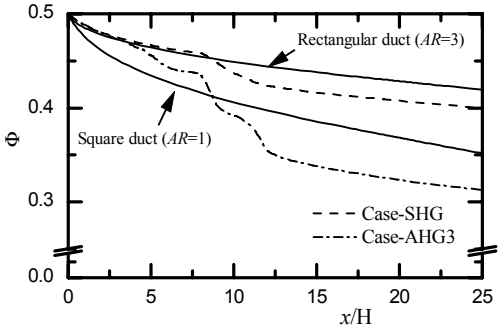

Fig. 12. Comparison of unmixed rate, Φ, between symmetric and asymmetric groove cases.

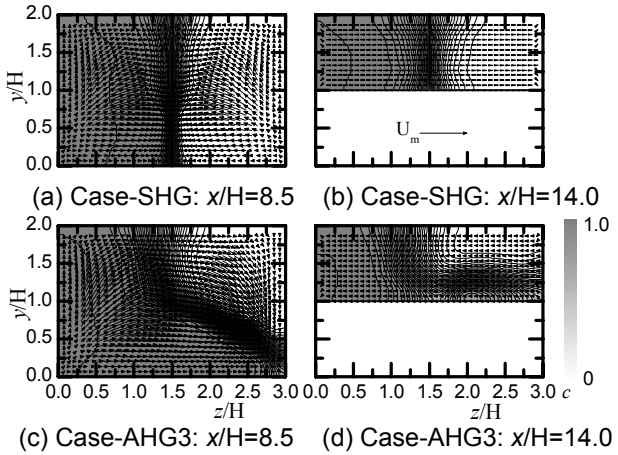

(a) Case-SHG: *x*/H=8.5 (b) Case-SHG: *x*/H=14.0

(c) Case-AHG3: *x*/H=8.5 (d) Case-AHG3: *x*/H=14.0

Fig. 13. Mixture fraction contours and velocity vectors in *y*-*z* plane at *x*/H=8.5 and 14.0 (grooved channels).

embedded grooves in the experimental and numerical cases are 30 and 5, respectively. *Re* is set as *Re*=1.5 in these cases.

Figures 7 and 8 show the streamwise velocity, *U*, contours on the *x*-*z* plane at *y*/H=0.26 and the cross-sectional distributions of the spanwise velocity, *W*, at three different spanwise locations, z/W_d=0.4, 0.5 and 0.6. Note that the results shown in each figure are obtained from the fourth groove counted from the upstream side of the channel. In Fig.7, the velocity contours of the two cases agree well. The *W* distributions of both results depicted in Fig. 8 also show a reasonable correspondence. These results evaluate the present numerical and experimental procedures for velocity measurements.

Figure 9 shows the cross-sectional distributions of the apparent mixture fraction, ϕ. ϕ is obtained by calculating the number density of the fluorescent particles in the experiment. In the numerical computation, this value is obtained by calculating the path lines of the particles injected from numerous locations at the inlet. In both cases, the results shown in Fig. 9 are obtained by spatially averaging the particle densities at *y*/H=1.5 in the streamwise direction in the area of one groove length (2*L*+*b* in Fig. 6) at the fourth groove. Furthermore, in the experiment, time-mean value is calculated by averaging 200 images of different time period. Although some discrepancy is observed at the maximum and minimum values, a good agreement is obtained for the location of each peak. Therefore, the apparent mixture fraction results obtained both by experiment and numerical simulation can be discussed in a qualitative way.

Discussion on Block-Inserted Channel

Figure 10 shows the streamwise distributions of the unmixed rate, Φ, of the block-inserted case under three different channel aspect ratio, *AR*, conditions obtained by the numerical computation. Φ is a dimensionless value defined as $\Phi = \int \rho u \xi dA/Q$. Here, ρ is the fluid density, *u* is the local streamwise velocity, and $\int dA$ is the integration in the cross-sectional plane. ξ is calculated as $\xi = |c - \bar{c}|$ where *c* is the mixture fraction of ethanol and $\bar{c}$ is the mixture fraction when the two fluids are completely mixed together, i.e. $\bar{c} = 0.5$. The results of the square (*AR*=1) and rectangular (*AR*=3) shape smooth channels are also shown in the figure for comparison. A smaller Φ is obtained by case-B1 and case-B3 compared to the smooth channel case of the same aspect ratio, which indicates a better mixing performance. Especially for case-B1, a noticeable enhancement is obtained. However, in the case of case-B3 when the channel aspect ratio is large, not much effect appears by inserted the blocks in the channel. Actually, a smaller Φ can be achieved by a smooth square channel case if the mass flow rate is the same as the present study.

Figure 11 shows the mixture fraction contours of the streamwise cross-sectional plane at *x*/H=6.5 (middle of the block streamwise length) of the block-inserted cases with different *AR*. Due to the block existence, the interface of the two fluids is distorted and expanded which results in an

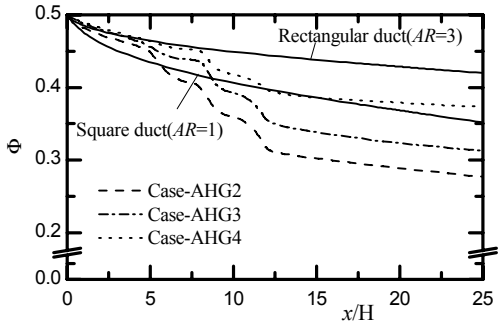

Fig. 14. Effect of channel aspect ratio on the unmixed rate, Φ, for grooved channel cases.

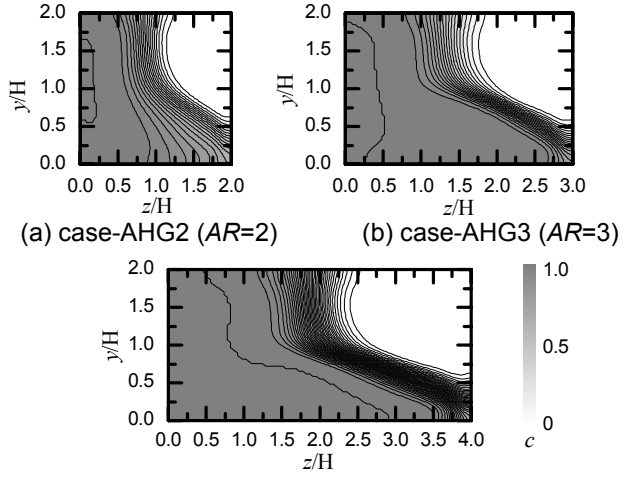

(a) case-AHG2 (*AR*=2) (b) case-AHG3 (*AR*=3)

(c) case-AHG4 (AR=4)

Fig. 15. Mixture fraction contours in *y*-*z* plane at *x*/H=8.5 (channel aspect ratio effect).

enhancement of the mixing performance. For larger *AR* cases, however, the interface per flow volume becomes small, and the influence of the block effect on the interface becomes relatively small. Therefore, it appears that the block-inserted cases are not effective in larger aspect ratio channels.

Discussion on Symmetric and Asymmetric Grooved Channels

Figure 12 shows the unmixed ratio, Φ, for case-SHG and case-AHG3. Same as Fig. 10, the results of the smooth channel cases are shown together in the figure. Comparing case-SHG with the smooth channels, case-SHG takes a smaller Φ than the rectangular duct case (AR=3), however, shows a larger Φ than the square duct (AR=1) case. On the other hand, Φ of case-AHG3 is smaller than the square duct case at the downstream of the groove.

Figure 13 shows the cross-sectional view of the velocity vectors and mixture fraction contours at *x*/H=8.5 and 14.0. From the velocity vectors at *x*/H=8.5, where the spanwise groove exists, generation of a secondary flow passing along the groove can be observed. Due to the convection produced by this secondary flow motion, the interface of the fluids is distorted and expanded. The fluid of higher or lower concentration is brought to the interface which increases the concentration gradient namely the diffusion flux at the interface. These are believed to be the reasons why a better mixing is obtained by the grooved channel cases. However, at *x*/H=14 the secondary velocity

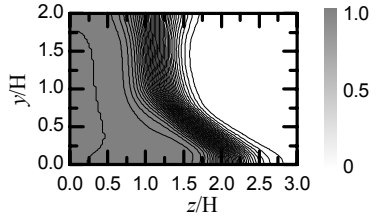

Fig. 16. Mixture fraction contours in *y*-*z* plane at *x*/H=8.5 of case-AHG3b.

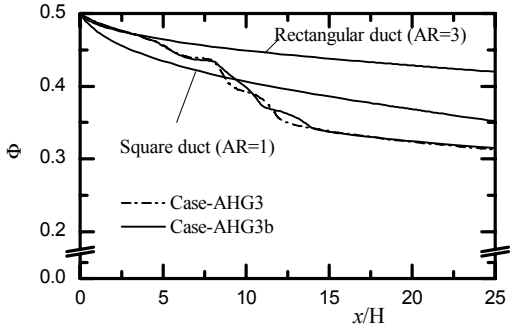

Fig. 17. Effect of spanwise groove width, *b*, on the unmixed rate, Φ.

components are small and the vortices do not maintain itself. The decrease ratio of Φ is, therefore, not large at the downstream of the grooves.

Under the condition of low Reynolds number as Re≈1, the secondary flow is relatively small for case-SHG, and a better performance is obtained by case-AHG3 which accompanies a surface extension effect of the interface additional to the increase of the diffusion flux at the interface.

Effects of Channel Aspect Ratio and Spanwise Groove Width

In this section, discussion is carried out on the *AR* and *b* effects on the flow and mixing characteristics of the asymmetric groove case. The streamwise distributions of Φ and mixture fraction contours at the cross-sectional plane of *x*/h=8.5 are respectively shown in Figs. 14 and 15 for the conditions of *AR*=2, 3 and 4. Same as the smooth channel case, Φ becomes smaller as *AR* increases since the interface becomes relatively small compared to the channel cross-sectional area. Focusing on case-AHG4, even though the aspect ratio is *AR*=4, Φ is equivalent to that of a square smooth channel, and is, furthermore, smaller than that of case-SHG or case-B2 whose aspect ratios are smaller (*AR*=3 or 2). This indicates that associated with the spanwise flow, mixing enhancement effect can be expected with the asymmetric groove case even for large channel aspect ratios.

Since the spanwise flow shows a significant contribution to the mixing characteristics as described above, the effect of the width of the spanwise groove, *b*, is discussed next. Fig. 16 shows the *c* contours of the *y*-*z* plane at *x*/H=8.5 of case-AHG3b whose *b* is three times larger than case-AHG3. In Fig. 17 is shown the Φ distributions of case-AHG3 and case-AHG3b. Comparing the results shown in Figs. 15 (b) and 16, one can see that the surface is distorted more in case-AHG3, which indicates that a stronger spanwise flow is produced at the

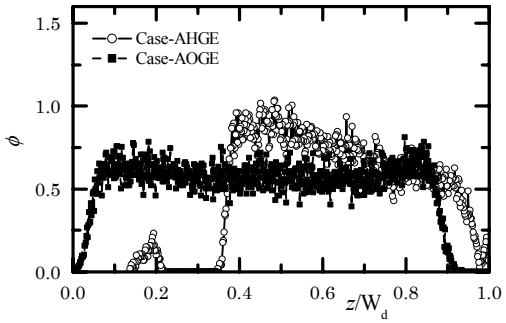

Fig. 18. Apparent mixture fraction, ϕ.

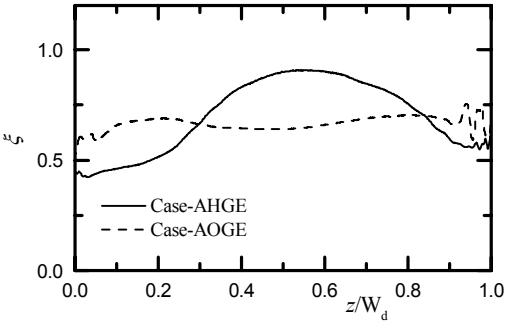

Fig. 19. Mixture fraction, ξ, obtained by measuring the fluorescence intensity of Rhodamine B.

spanwise groove and more fluid is transported from one side of the channel to the opposite side. By these effects, decrease of Φ shown in Fig. 17 is larger at 8<*x*/H<9 in this case than case-AHG3b. In case-AHG3b the interface is less expanded and the gradient of Φ is smaller at the same region. However, since *b* is increased the value decreases constantly in the area of 8<*x*/H<11 at which the spanwise groove is located. The contribution of these two effects to Φ, respectively appearing in case-AHG3 and case-AHG3b, are approximately the same. Therefore, consequently Φ at the downstream of the grooves are nearly identical and the difference of the mixing performance is small.

Comparison of Hook-Type and Oblique Grooves

In this section, discussion is carried out for the experimental results of the mixing characteristics of a hook-type asymmetric groove and oblique groove. Figures 18 and 19 show the cross-sectional distributions of the mixture fraction of each groove case. Figure 18 shows the apparent mixture fraction, ϕ, which is calculated by measuring the number density of the fluorescent particles at the plane of *y*/H=1.5. Figure 19 depicts the mixture fraction, ξ, calculated by measuring the fluorescence intensity at the same location. Both values are spatially averaged in the streamwise direction for one groove length (=2*L*+b) and time-averaged by averaging the data of 200 images. Comparing ϕ and ξ for case-AHGE, although both values are calculated at the same streamwise location, ξ has a smoother distribution compared to that of ϕ. This is believed to be ascribable to the diffusion effect of Rhodamine B and to the fact that the measured fluorescence intensity is the summation of the light in the depth direction. Nevertheless, the characteristics of each distribution roughly agrees with each other, at least in a qualitative sense.

Comparing the results of case-AHGE and case-AOGE, a more uniform distribution is obtained by case-AOGE for both ϕ and ξ which indicates that a better mixing is produced by this case. Although not shown here, the flow rate in the groove in the spanwise direction in case-AOGE is larger than case-AHGE which indicates a larger fluid transport resulting in a mixing enhancement. It is believed that the increase of the spanwise flow is attributed to the inclination of the groove and to the increase of the groove width.

CONCLUSIONS

Flow and mixing characteristics of a micro-channel with blocks and grooves applied to the walls have been discussed by numerical and experimental approaches. The major conclusions drawn from the present study is as follows:

1. The results of the velocity fields measured by the μ-PIV for the flow in a rectangular smooth channel showed an excellent agreement with the three-dimensional analytical results. The apparent mixture fraction obtained by measuring the number density of the fluorescent tracing particles in the grooved channel corresponded fairly well with the results of the numerical simulation.
2. In the case of the block-inserted channel, a good mixing was obtained for the square channel. However, the performance significantly deteriorated as the channel aspect ratio (*AR*) increased indicating that the block-inserted case is not effective for channels of large *AR*.
3. For the case of grooved channel, an effective mixing was obtained even when *AR* is large. The grooved channel of *AR*=4 produced a comparable performance to the square smooth channel and block-inserted case of *AR*=2.
4. Comparing the performances of the grooves of symmetric and asymmetric patterns, a better mixing was obtained by the asymmetric groove case. This is ascribable to the spanwise flow which distorted and expanded the interface of the two fluids.
5. Under the condition of the present study, the width of the spanwise groove consequently did not affect the mixing performance if compared at the downstream of the groove. This is due to the trade-off problem between the increase of the area of larger fluid mixing, and the enhancement of spanwise fluid transport produced by the groove.
6. Comparing the results of the hook type asymmetric groove and the oblique groove cases, the latter case showed a better performance.

REFERENCES

1. C. D. Meinhert, S.T. Wereley and M. H. B Gray, Volume illumination for two-dimensional particle image velocimetry, Measurement Science and Technology 11, 809-814 (2000).
2. D. G. Drake, On the Flow in a Channel due to a periodic pressure gradient, Quarterly J. of mechanics and applied mathematics, 18, 1-10 (1965).

ACKNOWLEDGEMENT

The work is partially supported through the project "MEMS Open Network Engineering System of Design Tools (MEMS-ONE)" by Micromachine Center (MMC).